Dynamic coordination process between a triphenylamine-functionalized salicylaldehyde Schiff-base and copper (II) ion

Xing Zhang,[a] *Shou-Ting Wu,* [b] *Xian-Jiong Yang,* [b] *Ling-Yi Shen,* [b] *Ya-Li Huang,* [b] *Hong Xu,* *[b] *Qi-Long Zhang,* *[b] *Tao Sun,* [c] *Carl Redshaw*[d] *and Xing Feng,* *[e]

[a]School of Public Health, the key Laboratory of Environmental Pollution Monitoring and Disease Control, Ministry of Education, Guizhou Medical University, Guiyang 550025, China.

[b] School of Basic Medical Sciences, Guizhou Medical University, Guiyang 550025, China.E-mail：xuhong@gmc.edu.cn or gzuqlzhang@126.com.

[c] Key Laboratory of Macrocyclic and Supramolecular Chemistry of Guizhou Province, Guizhou University, Guiyang, Guizhou 550025, China

[d] Department of Chemistry, University of Hull, Cottingham Road, Hull, Yorkshire HU6 7RX, UK

[e] Guangdong Provincial Key Laboratory of Functional Soft Condensed Matter, School of Material and Energy, Guangdong University of Technology, Guangzhou 510006, P. R. China. E-mail: hyxhn@sina.com.

ABSTRACT: The coordination between a ligand and a metal is a spontaneous and uncontrollable process. In this article, we successfully observe the formation process of metal coordination in a triphenylamine-functionalized salicylaldehyde Schiff-base with copper (II) ion. The ligand **TPA-Py** firstly reacts with Cu^{2+} in a step-wise process to afford the dynamic complex **TPA-Py@Cu^{2+}** ([ligand]:[Cu^{2+}] = 1:1), which further reacts with an extra copper(II) ion to afford **2TPA-Py@4Cu^{2+}** with step-wise (or cumulative) stability constants of $K_1 = 4.0694 \times 10^3$ and $K_2 = 1.0761 \times 10^6$, respectively. The entire metal coordination process can be visualized and the coordination mode of the probe towards copper was further evaluated by UV-vis/fluorescence spectra, single crystal X-ray diffraction, DFT calculations, HRMS spectra, as well as by NMR spectroscopic titrations. The compound **TPA-Py** exhibited excellent sensitivity and specificity toward copper (II) ions in THF/water media with a low limit of detection of 2.687×10^{-7} mol L^{-1}. In addition, **TPI-An-Py** can be applied to the detection of Cu^{2+} in real samples with satisfactory recoveries in the range of 100%~112% in lake water and 98%~101% in tap water. This article not only reports an excellent fluorescence probe for copper (II) ion detection, but also presents an instance for more fully understanding the metal coordination process.

1. INTRODUCTION

The physiological role of Cu^{2+} is crucial in maintaining the body's hematopoietic function, and keeps the central nervous system in good condition, and it also acts as a coenzyme for many enzymes.[1, 2] Lack or excess of copper in living organisms can cause many health disorders, such as anemia, hypercholesterolemia, anorexia, jaundice, hemolytic and other diseases.[3, 4] Thus, the development of technologies for copper ion detection has become an important focus in environmental and food nutritional fields. The traditional methods include atomic absorption

spectroscopy, ion chromatography, gas chromatography-mass spectrometry (GC-MS) and inductively coupled plasma mass spectrometry (ICP-MS),[5, 6] which have been widely utilized for detecting Cu^{2+}, but such systems still have their limitations such as the need for large and expensive instruments, complex modes of operation and high detection costs, etc. In recent years, methods based on fluorescent probes have emerged as the cutting-edge technology in the field of metal ion detection due to convenient procedures, super-sensitivity, and fast response times.[7, 8]

Most traditional fluorescent materials exhibit an aggregation caused quenching (ACQ) effect, which means that they are highly emissive in solution, but a quenching affect exists in the aggregation state. In the case of dyes, the ACQ effect can greatly limit their practical applications in material science.[9] In contrast, an abnormal photophysical phenomenon was observed by Tang's group in 2001,[10, 11] namely aggregation induced emission (AIE), whereby the fluorescent molecules exhibit non-/weak emission in solution but enhanced fluorescence in the aggregation state, and the accepted mechanism of AIE involves restriction of intramolecular motions (RIM). Molecules emit energy through intramolecular rotation and vibrational motions in the solution, while in the aggregation state the non-radiative transition is blocked, and in turn energy is lost through the radiative transition channel.[12]

Besides the AIE phenomenon, excited state intramolecular proton transfer (ESIPT) is also a significant luminescence mechanism. Probes with ESIPT process will lead to a uniquely large Stokes shift, which attributes to a very fast photo-tautomerization transformation from enol form to keto form when the molecules contain an active phenolic hydroxyl.[9, 13-16] More importantly, fluorescent dyes with the ESIPT property have clearer changes of optical phenomenon in their solutions which can be directly observed by the naked-eye.[17-19] Novel fluorescent probes bearing

AIE plus ESIPT features would lead to a large Stokes shift with limited self-quenching emission, considerable hydrophilicity, as well as high signal-to-noise ratio, etc.[20]

On the other hand, understanding the self-assembly or coordination processes between a host and a guest is vital to prepare the ideal metal-organic frameworks (MOFs) or covalent organic frameworks (COFs) with suitable size-dependent nano materials for potential application in energy gas storage, (heavy) metal ions capturing, as well as for biosensors.[21-26] In fact, a coordination reaction between a host ligand and a guest is a dynamic and concentration-dependent process, but is typically an uncontrollable process, which leads to a stable self-assembled architecture. It is difficult to observe these dynamic reactions[27, 28] in common chemical reactions.

Herein, a new triphenylamine-functionalized salicylaldehyde Schiff-base fluorescent probe possessing ESIPT and AIE characteristics was designed and synthesized based on our previous research.[29] The recognition performance of the probe toward Cu^{2+} ions was excellent with a low limit of detection of 2.687×10^{-7} mol·L^{-1}. Moreover, the coordination mode of the probe with copper (II) was investigated by ^{1}H NMR spectroscopic titrations and by single crystal X-ray diffraction. The information gleaned from the studies herein sheds light on the coordination process of this system, and will help future design strategies for AIE gens for practical use.

2. EXPERIMENTAL SECTION

2.1 Materials and Characterization

Unless otherwise stated, all of the starting materials were commercially available and used without further purification. The solution of metal ions and anions were prepared from their nitrate and sodium salts, respectively. ^{1}H NMR spectra (400 MHz) were recorded on a Inova-400

Bruker AV 400 spectrometer using d-DMSO solvent and tetramethylsilane as the internal reference. J-values are given in Hz. High-resolution mass spectra (HRMS) were recorded on a GCT premier CAB048 mass spectrometer operating in a MALDI-TOF mode. UV-vis absorption spectra were obtained on a UV-2600 Milton Ray Spectrofluorometer. PL spectra were recorded on a Cary eclipse spectrofluorometer.

2.2 Synthesis of Compound TPA-Py

A mixture of 4'-(di-p-tolylamino)-3-hydroxy-[1,1'-biphenyl]-4-carbaldehyde (79 mg, 0.2 mmol) and *N, N′*-(2-aminophenyl)-2,6-dicarboxylimide pyridine[29] (35 mg, 0.1mmol) was dissolved in 20 mL methanol and stirred at room temperature 5 min., then 10μL H_2SO_4 was added into the mixed solution and stirred for 7h. The precipitate was filtered and washed with hot methanol for three times, and dried in vacuum to obtain the target compound **TPA-Py** (83 mg, yield 76 %) as a yellow solid. ^{1}H NMR (400 MHz, DMSO) δ 13.04 (s, 2H), 10.61 (s, 2H), 8.52 (d, *J* = 7.7 Hz, 2H), 8.43 – 8.36 (m, 1H), 8.31 – 8.21 (m, 4H), 7.49 (d, *J* = 8.2 Hz, 2H), 7.34 – 7.23 (m, 4H), 7.17 (d, *J* = 8.4 Hz, 12H), 7.08 – 6.95 (m, 12H), 6.89 (d, *J* = 8.6 Hz, 4H), 6.44 (s, 2H), 2.30 (s, 12H) ppm. ^{13}C NMR (101 MHz, $CDCl_3$) δ 161.92, 161.09, 159.99, 149.84, 148.68, 145.21, 145.01, 138.83, 133.17, 132.14, 131.96, 130.11, 127.74, 126.35, 125.93, 124.98, 124.59, 121.97, 117.83, 117.07, 116.51, 114.20, 20.99. HR-MS calculated for $[M]^+$ 1098.4662, found 1098.4712.

2.3 General Methods for Optical Test

Probe **TPA-Py (**11mg) was dissolved in 10.00 mL THF solution to obtain stock solution (10μM). Then the nitrates of metal ions and the sodium salts of the anions (Ag^+, Al^{3+}, Ba^{2+}, Cd^{2+}, CO^{2+}, Cr^{3+}, Na^+, Cu^{2+}, K^+, Ni^{2+}, Pb^{2+}, Zn^{2+}, Hg^{2+}, Fe^{3+}, Mg^{2+}, Li^+, AcO^-, HSO_3^-, Cl^-, Br^-, I^-, F^-,

SO_4^{2-}, NO_2^-, ClO_4^-, $H_2PO_4^-$, PO_4^{3-}, HCO_3^-, HPO_4^{2-}, $C_2O_4^{2-}$, SO_3^{2-}, CO_3^{2-}) were accurately weighed and dissolved in 10.00 mL Tris-HCl buffer to form the ion stock solution (10mM). Unless otherwise stated, the entire analytic experiment was carried out by using these stock solutions mentioned above. The given aqueous condition was prepared with Tris-HCl buffer. The preparation method of Tris-HCl buffer solution (2 mM) was as follows: 121.20 mg of trimethylol aminomethane was dissolved in 1.00L ultrapure water, then its pH was adjusted to 7.00 with 0.10M HCl solution and 0.10M NaOH solution.

2.4 X-ray Crystallography

Crystallographic data for ligand **TPA-Py** was collected on a Bruker APEX 2 CCD diffractometer with graphite-monochromated Mo K_α radiation (λ = 0.71073 Å) in the ω scan mode.[30] The structures were solved by a charge flipping algorithm and refined by full-matrix least-squares methods on F2.[31] All esds were estimated using the full covariance matrix. Further details are presented in Table S1. Data for the structures reported here have been deposited with the Cambridge Crystallographic Data Centre with deposition numbers CCDC 2052956 for **TPA-Py@Cu^{2+}**, 2052957 for **2TPA-Py@4Cu^{2+}** and 2052958 for **TPA-Py**, which contain the supplementary crystallographic data for this paper. These data can be obtained free of charge from The Cambridge Crystallographic Data Centre via www.ccdc.cam.ac.uk/data_request/cif.

2.5 Preparation for Water Sample Test

A 7.8 mL THF solution, 200 μL probe stock solution (20 μM), 1 mL Tris-HCl buffer and 1 mL water sample (had been filtered) were added into several volumetric flasks and shaken well. At the same time, another water sample was prepared using the same procedure but an appropriate amount of the standard substance ($Cu(NO_3)_2$) was added. After standing for 30 min, we firstly tested the sample without $Cu(NO_3)_2$ and obtained the "measured" data, then, the

specimen which containing the standard substance was further studied and recorded. By comparing the data with and without the standard substance, the recovery rate of the sensing experiment could been calculated.

3 RESULTS AND DISCUSSION

3.1 Synthesis and characterization of the target compound TPA-Py

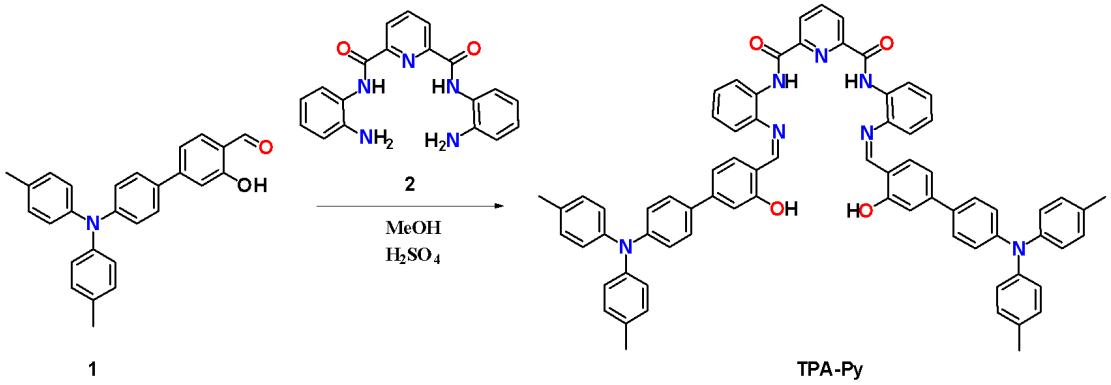

Scheme 1. Synthetic route to Schiff-base **TPA-Py.**

The compound **TPA-Py** was synthesized according to the previously reported method,[29] and this is outlined in Scheme 1. **TPA-Py** was fully characterized by ^{1}H NMR spectroscopy, single crystal X-ray diffraction and High-Resolution Mass Spectrometry (HRMS). The Schiff-base exhibited excellent solubility in common organic solvents (such as toluene, tetrahydrofuran and dimethyl sulfoxide, etc.) and possessed good acid and alkali-resistance over the pH range 3 - 11 within 24h (Fig.S7).

3.2 AIE properties

Previously, our group reported a related tetraphenylethylene-functionalized salicylaldehyde Schiff-base compound, which exhibited AIE characteristics with red emission.[29] Here, the AIE properties of the Schiff-base **TPA-Py** have been investigated in dilute THF and THF/water

mixtures with various water fraction (f_w) at room temperature. As shown in Fig.1, the compound **TPA-Py** emitted bright yellow emission with $\lambda_{em(max)}$ = 576 nm in pure THF solution. As the water fraction (f_w) increased from 0% to 10%, the fluorescence intensity dropped rapidly. Following that, when the water fraction increased from 10% to 50%, the emission intensity of the mixture gradually decreased, and this may be attributed to the ESIPT effect. According to the literature,[32] probes with intramolecular H-bonding usually undergo a fast four-level (Enol-Enol*-Keto*-Keto) after luminescence excitation,[16] which will lead to a "double fluorescence" (enol emission and keto emission) phenomenon. When the recognition environment contains a protonic polar solvent like H_2O, the intramolecular H-bonding can become intermolecular H-bonding between the **TPA-Py** and H_2O. As a result, the ESIPT process was blocked and the fluorescent intensity at the emission peak dropped sharply. [33] Subsequently, when f_w increases to more than 50%, the solution containing **TPA-Py** began to appear turbid and the emission was enhanced due to molecular aggregation. When f_w reached 95%, the fluorescence intensity of the solution attained the maximum value with an approximate 1.2-fold increase *versus* that in pure solution. The quantum yield in the solid state (Φf=18.6 %) is higher than that in THF solution ((Φf= 16.9%). Thus, the Schiff-base **TPA-Py** exhibited a clearly aggregation-induced emission characteristic.

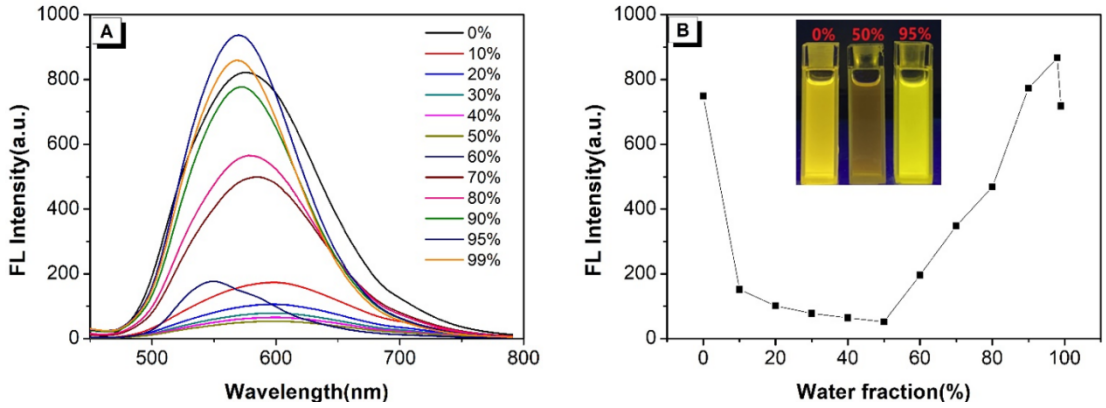

Fig.1. (A) Fluorescence spectra of **TPA-Py** (2.00×10^{-5} mol $\cdot L^{-1}$) in THF/water mixtures with different water fractions (λ_{ex}= 425 nm, slit: 5/5 nm, voltage: 680 v). (B) Fluorescence intensity (λ_{em} =598 nm) plots of TPI-An-Py in THF/water mixtures with different water fractions. Insert: photograph of the probe solution with water fraction of 0%, 50% and 95% under a 365 nm UV lamp.

3.3 Solvatochromic effect

The solvatochromic effect of **TPA-Py** was investigated in some non-polar and polar solvents with the concentration of **TPA-Py** remaining constant. As the polarity increased, the emission displayed a red-shift of about 50 nm in THF (λ_{em} = 576nm) compared to hexane (λ_{em} = 525nm) and the emission color turned from green to orange/red depending on the polar solvent employed. Thus, the solvent polarity plays a significant role on the emission (fig.2A and 2B) and absorbance (Fig S6) behavior.

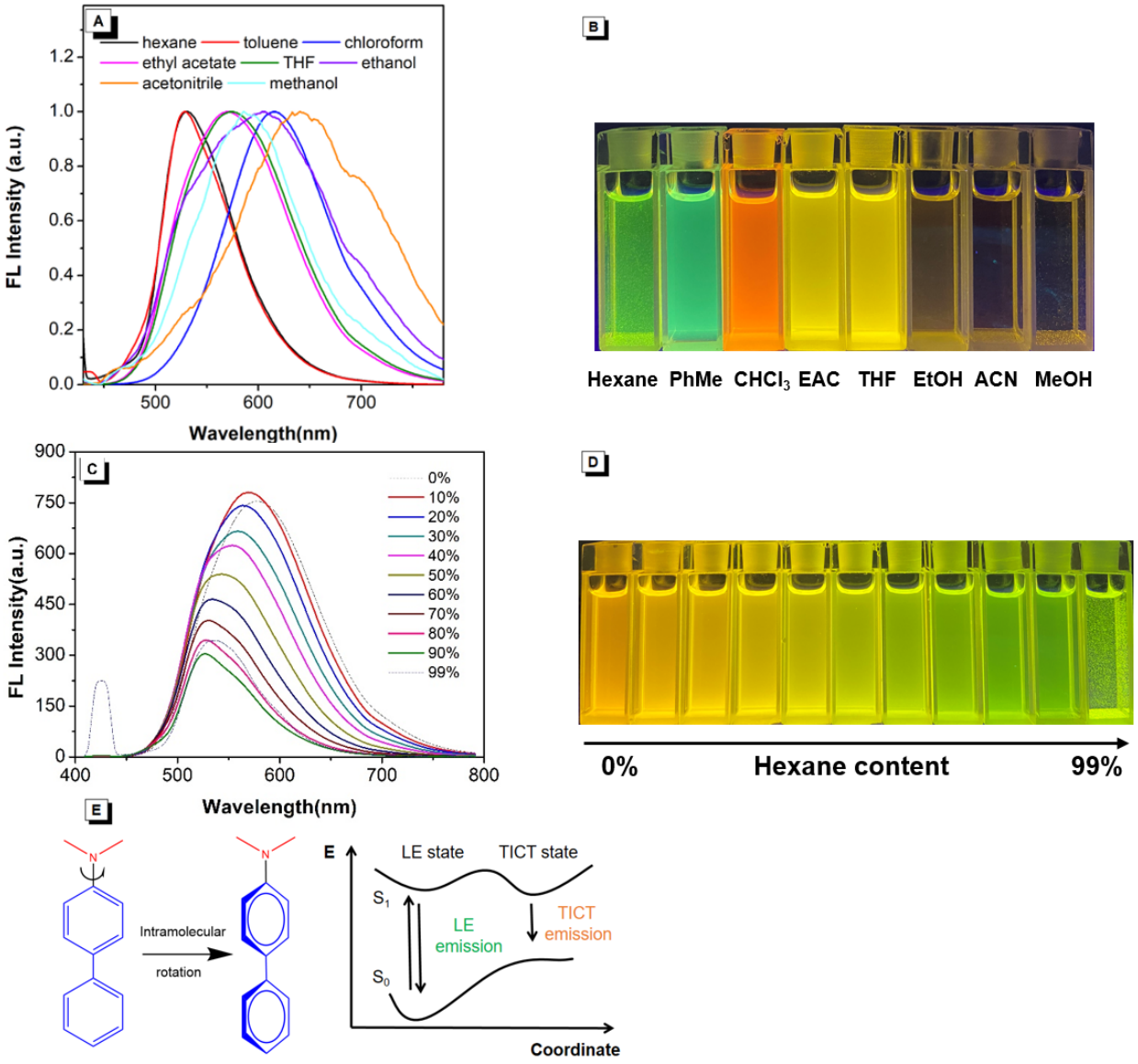

Fig. 2. (A) The fluorescence spectra of the probe in various polar solvents. (B) The fluorescence images of the probe in hexane, toluene, chloroform, ethyl acetate, THF, ethanol, acetonitrile and methanol recorded under a 365 nm UV lamp. (C) The fluorescence spectra of **TPA-Py** in tetrahydrofuran solution with different contents of hexane (λ ex= 425 nm, slit: 5/5 nm, voltage: 680 v). (D) Fluorescence photos of the probe in a hexane-tetrahydrofuran mixture with different hexane content (0% ~ 99%) under a 365 nm UV lamp. (E) Transition of the locally excited (LE) state of **TPA-Py** to the twisted intramolecular charge transfer (TICT) state through intramolecular rotation of its donor (D) and acceptor (A) units in the excited state.

To more deeply understand the relationship between the polarity of the solvent and the emission spectra, the fluorescence spectra of the **TPA-Py** were investigated in dilute THF and THF/hexane mixtures with various hexane fraction (f_h) added. As shown in Fig.2, with the

increase of the f_h from 0 to 99%, the maximum emission peak of the **TPA-Py** gradually blue shifted from λ_{em} = 576 nm in THF to 525 nm in hexane along with a decrease in fluorescence intensity, accompanied with a new shoulder peak at λ_{em} = 426 nm. The long wavelength emission originates from the keto emission and the short wavelength emission is attributed to the enol peak.

In the **TPA-Py** system, the triphenylamine unit act as a strong electron-donating group, and the *N,N′*-(2-aminophenyl)-2,6-dicarboxylimide pyridine units as an electron-withdrawing group. Thus, we propose that the luminescent behavior of the bipolar molecule **TPA-Py** is mainly affected by the locally excited (LE) state in non-polar solvent. As the solvent polarity increases, the molecular structure becomes more planar via an intramolecular rotational motion process. The interaction between polarized molecules and surrounding solvent molecules will be enhanced by the increase of solvent polarity. When the D - π - A molecules are excited by light, the electrons will transfer from the donor to the receptor units, resulting in a D^{+}* -π- A^{-}* state (TICT state). Compared with the ground state, the excited luminogen has a larger dipole moment, so the polar solvent is more stable for the TICT state. In addition, the TICT state has a smaller energy gap than the LE state, and this may lead to a red-shifted emission with an increase of solvent polarity.[34-36] On the other hand, when the polarity of the mixture slowly decreases, there is tendency towards diminished emission intensity. The possible reason may be that the solvent polarity can strongly affect the emission behavior of the ICT molecules. [37, 38] Under irradiation, the strong polar solvent is beneficial for the stabilization of the excited molecules by enhancing the dipole moment of the polar molecules, which leads to a suppression of the non-radiative transition process. While in the nonpolar solvent, such as hexane, the incompatible molecular polarity between solvent and solute will exhaust more excited energy,[39] resulting from

a decreased fluorescent intensity in hexane compared in THF solution. On the other hand, as the solvent polarity increased from ethanol, acetonitrile to methanol, the emission intensity drops dramatically, this may be attributed to the stronger intramolecular charge transfer process leading to fluorescence quenching.[40]

3.4 Cation sensing study

Schiff base compounds are widely used in the recognition of rare-earth metals, transition metals and alkali metals as a result of their high binding affinity.[41, 42] To test the detecting capacity toward metal ions, the probe **TPA-Py** (2.00×10^{-5}mol/L) with twice as many metal ions (such as K^+, Hg^+, Cd^{2+}, Al^{3+}, Ba^{2+}, Li^+, Na^+, Cu^{2+}, Mg^{2+}, Cr^{3+}, Ni^{2+}, Fe^{3+}, Zn^{2+}, Ag^+, Co^{2+}, Pb^{2+}, $[M]^{n+}=4.00\times10^{-5}$ mol $\cdot L^{-1}$) were evaluated in mixtures of THF and water (V_{THF} /V_{H2O} =4/1, pH = 7.00).

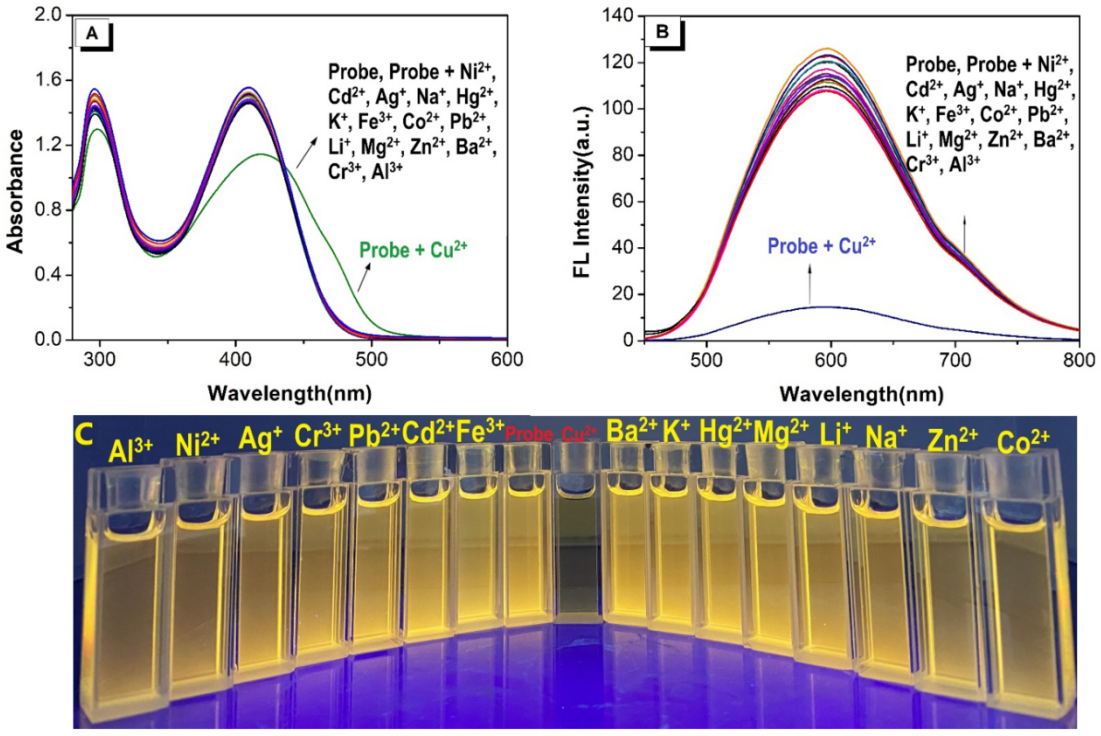

Fig.3. (A) The UV-vis and (B) Fluorescence spectra of the fluorescence probe **TPA-Py** (2.00×10^{-5} mol $\cdot L^{-1}$, V_{THF}:V_{H2O} = 4/1, Tris-HCl buffer 2.00×10^{-3} mol $\cdot L^{-1}$, pH = 7.00) interacting with different metal ions (4.00×10^{-5} mol $\cdot L^{-1}$)($\lambda_{ex}/\lambda_{em}$ = 415/598 nm, slit: 5/5nm, voltage: 900 v). (C) Photograph of **TPA-Py** interacting with metal ions under a 365 nm UV lamp.

As shown in Fig. 3, on adding the metal ions to the solvent containing **TPA-Py**, only Cu^{2+} can cause the solution color to change via naked-eye observation. The absorption spectra of **TPA-Py** indicated that the maximum absorption peak changed from 409 nm to 418 nm. Moreover, the emission peak at 598 nm decreased dramatically in the presence of copper ions, while other metal ions had only a limited effect on both the absorption and fluorescence behavior (Fig.3A and 3B). Various anions were utilized to test the selectivity of **TPA-Py** and the spectra of the mixtures remained almost unchanged (Fig.S8). Thus, the Schiff-base **TPA-Py** can be utilized as an excellent fluorescence probe for detecting Cu^{2+}. Compared to reported Cu^{2+} sensors, (Table S2), this present system utilizing **TPA-Py** shows many advantages, such as wide applied pH range, controllable emission properties and a low detection limit. In addition, the fluorescence quenching is mainly due to the intramolecular charge transfer (ICT) from the triphenylamine units to the Cu^{2+} when the copper ion interacts with **TPA-Py.**[36]

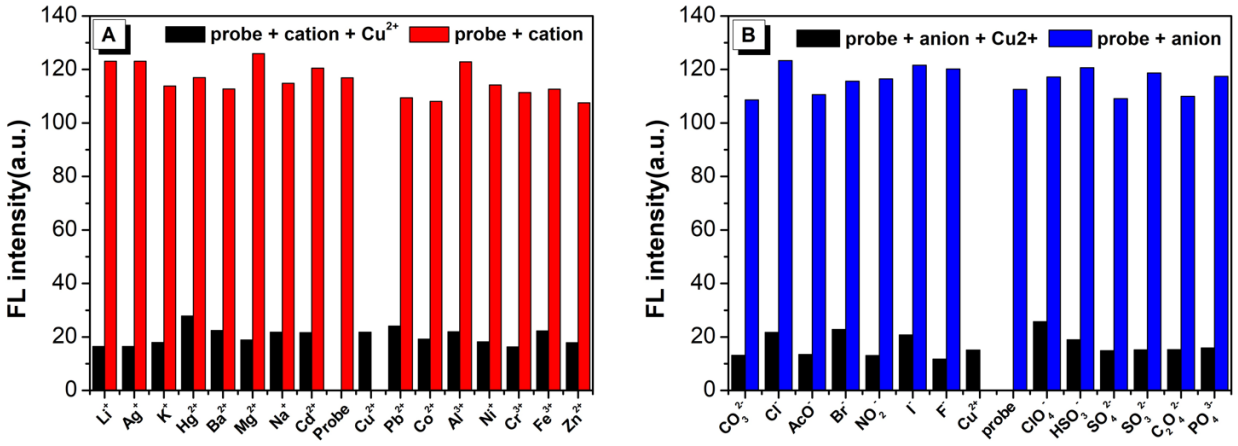

Fig.4. Bar diagram of the competitive experiments of various metal cations (A) and anions (B) on the fluorescence intensity of the probe/Cu^{2+} complex in buffer solution (λ ex/ λ em= 425/598 nm, slit: 5/5 nm, voltage: 680 v).

Competitive experiments were performed to study the selective recognition ability of the probe toward Cu^{2+}. Herein, to the solution containing **TPA-Py** and Cu^{2+} was added 10 equiv. of

other coexisting ions (such as Hg^{2+}, Ag^{+}, Li^{+}, Ca^{2+}, Ba^{2+}, Al^{3+}, K^{+}, Na^{+}, Mg^{2+}, Zn^{2+}, Cr^{3+}, Fe^{3+}, Pb^{2+}, Cd^{2+}, Co^{2+}, Ni^{2+}, ACO^{-}, ClO_4^{-}, Br^{-}, NO_2^{-}, CO_3^{2-}, I^{-}, F^{-}, SO_4^{2-}, Cl^{-}, $H_2PO_4^{-}$, PO_4^{3-}, HPO_4^{2-}, $C_2O_4^{2-}$, SO_3^{2-}, HSO_3^{-}, HCO_3^{-}). When Cu^{2+} was present in the solution, the emission peal at λ_{em} = 598 nm was dropped dramatically, while without the presentation of Cu^{2+}, the fluorescent intensity of the mixture almost unchanged (Figure 4), which demonstrated that the coexisting cations/anions had less impact on the recognition of Cu^{2+}. Basing on the above experiments, we confirm the probe **TPA-Py** exist a high specificity and selectivity towards Cu^{2+} recognition.

3.5 Coordination mode

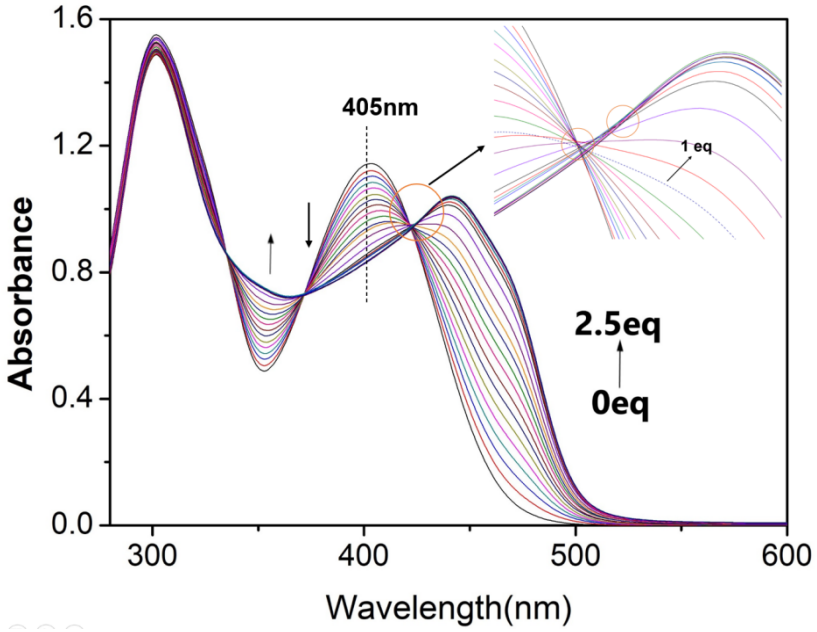

Fig.5. The change of absorbance spectra on addition of 0 - 2.5 equiv. of Cu^{2+} to the probe. insert: the detail image of the absorption band from 410 nm to 445 nm.

Absorption experiments were carried out in order to understand the stoichiometric ratio between the ligand **TPA-Py** and Cu^{2+}. As shown in Fig. 5, it was found that the absorbance peak at 405 nm decreased gradually as the Cu^{2+} was added over the range 0-1.0 equivalents with a clear isoabsorptive point at 423 nm.

Further, the binding mode of probe **TPA-Py** and Cu^{2+} was investigated by a Job's plot by controlling the total concentration of the probe and Cu^{2+} at 2.00×10^{-5} mol L^{-1} in a mixture of THF/H_2O (V_{THF}/V_{H2O} = 4/1). The results indicated that the binding stoichiometry between the probe and Cu^{2+} was 1:2 (Fig. S9). Based on the results of the titration experiments, a plot of correlation curve was calculated (Fig. S10). According to the formula:[43]

$$\Delta A = \frac{k_{\Delta HG}[\mathrm{H}]_0 K_1[\mathrm{G}] + k_{\Delta HG2}[\mathrm{H}]_0 K_1 K_2[\mathrm{G}]^2}{1 + K_1[\mathrm{G}] + K_1 K_2[\mathrm{G}]^2}$$

Here, ΔA is the difference between the absorbance intensity at 442 nm in the presence/absence of Cu^{2+}, $[H]_0$ is the total concentration of the **TPA-Py**, [G] is the free (unbound) concentration of the Cu^{2+}, [HG] is the concentration of the complex [**TPA-Py@Cu**]. We utilized the **KaleidaGraph** Version 4.0 to calculate the binding constant (K_a) between the probe (**TPA-Py**) and the Cu^{2+} to be $K_1 = 4.0694 \times 10^3$ and $K_2 = 1.0761 \times 10^6$. On the basis of this work, the detection limit was calculated by utilizing the data of the fluorescence titration experiments following the IUPAC method[44]: 10 groups of blank samples were tested in the absence of copper under the same conditions, and then the standard deviation (SD) was calculated from the emission peak at 598 nm. According to the formula: the detection limit = 3SD/S, where S is the slope of the linear relationship during the fluorescence titration, namely the slope of the correlative equation obtained in the titration experiment mentioned above (Fig. S10), following that, the detection limit of probe **TPA-Py** for Cu^{2+} is calculated to be 2.687×10^{-7} mol $\cdot L^{-1}$.

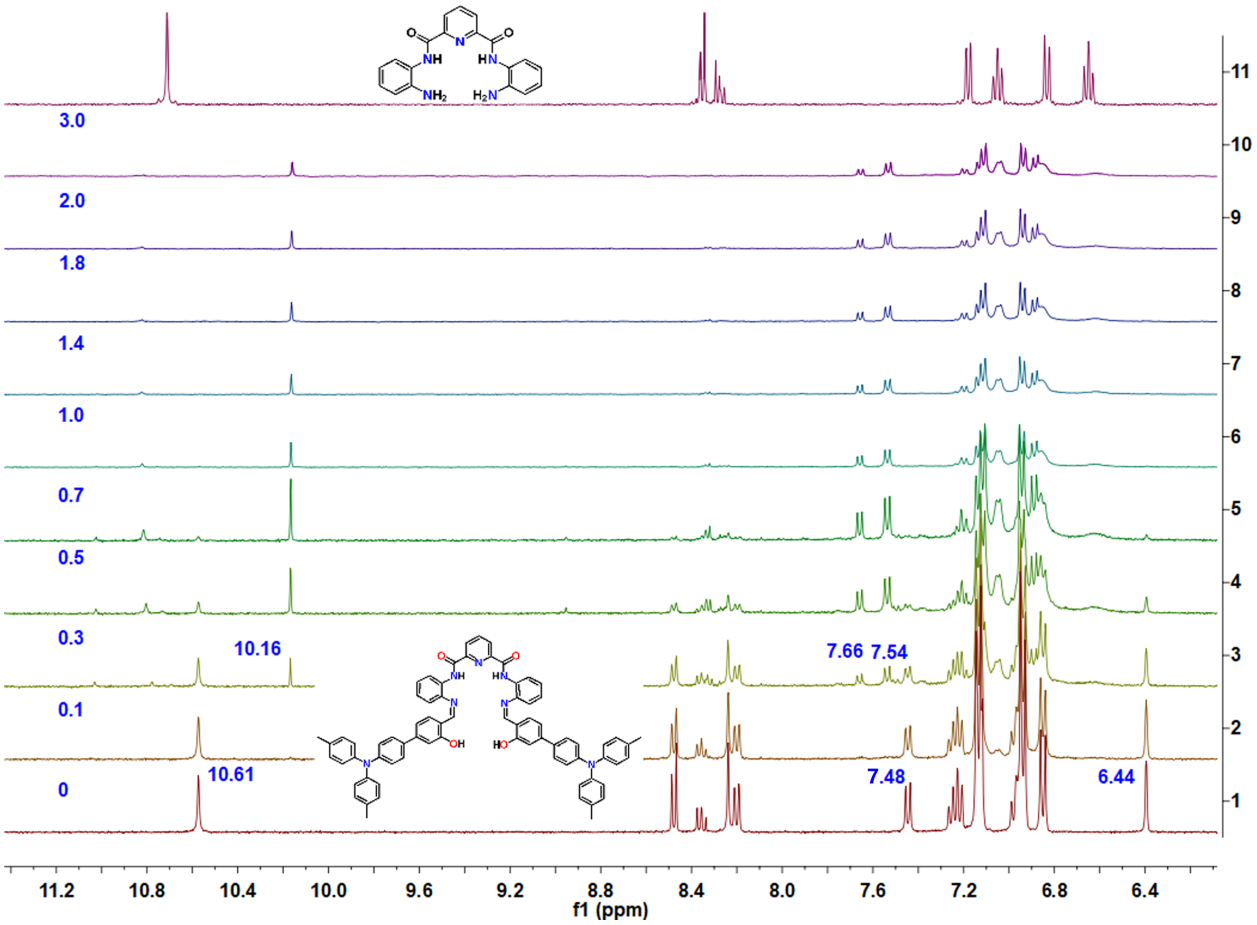

Fig. 6. ^{1}H NMR spectroscopic titration spectra of the mixture on increasing the stoichiometric ratio of **TPA-Py**: Cu^{2+} (0, 0.1, 0.3, 0.5, 0.7, 1.01, 1.4, 1.8, 2.0, 3.0 eq.) in d-DMSO solution.

To better understand the recognition mechanism of **TPA-Py** for detecting copper ions, ^{1}H NMR spectroscopic titration experiments in d-DMSO solution were performed. According to Fig. 6, four groups of singlets (δ = 13.04, 10.61, 8.29 and 6.44 ppm) were observed for the –OH, –CO-NH-, –CH=N and phenyl ring, respectively. A doublet (δ = 8.52 ppm, J = 8 Hz) and a triplet peak (δ = 8.40 ppm) was observed for the pyridine ring. The proton peak at δ = 8.24 (J = 8 Hz), 7.48 (J = 8 Hz), and 7.24-7.30 ppm are assigned the bridge of diphenylamine ring, and the three groups of doublet peaks at δ = 7.17, 6.98 and 6.89 ppm are from the triphenylamine, respectively. Additionally, the proton peak from the bridge of the diphenylamine and salicylaldehyde units are overlapped and also located at δ = 7.24-7.30 and 6.98 ppm, respectively. Upon addition of 0.3 equiv. of Cu^{2+} to the probe solution, the proton signal at δ

13.04 (–OH) disappeared and two new singlet proton peaks at 10.80 and 10.16 ppm appeared, and the proton resonances of the bridge of diphenylamine ring (δ= 7.48 ppm) split into two doublets at δ = 7.66 and 7.54 ppm, indicating that the Cu^{2+} had connected with the O and N atom from the hydroxyl group and the –C–NH–C=O fragment, respectively. On slowly increasing the amount of Cu^{2+} from 0.3 to 3 equiv., the proton peak in range from 8.43-8.21 ppm, 7.45 ppm and a singlet peak at 6.44 ppm gradually disappeared, while the single proton peak at 10.80 ppm enhanced then gradually disappeared, indicating that the copper (II) can coordinate with the TPA-Py.

3.6 X-ray single crystal diffraction analysis

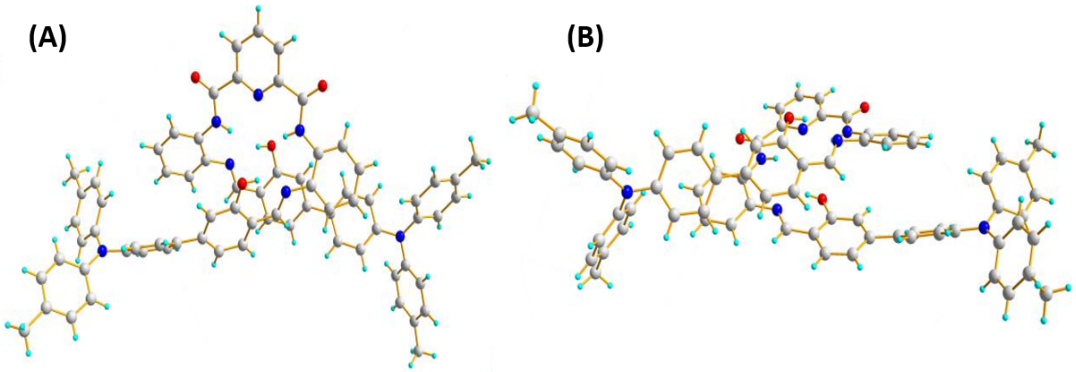

Fig. 7. The X-ray single crystal diffraction image of **TPA-Py** in front (A) and side(B) views.

A suitable single crystal of **TPA-Py** was cultivated from a mixture of dichloromethane and methanol by slow evaporation, and an X-ray diffraction analysis was performed. The crystal **TPA-Py** belongs to the triclinic space group P-1. As shown in Fig. 7, the fragment containing the biphenyl amine units as arms were crossed in front of the bridging pyridyl unit, and the 3D twist molecules form a helical conformation,[45] similar to our previous report.[29] In addition, two groups form weak intermolecular interactions, namely an O-H···N bond (O1-H1···N5 = 1.886 Å and

O19-H19···N13 = 2.027 Å) were observed. The compound **TPA-Py** is an excellent ligand for coordinating with copper (II) ions via the N- and O- atoms.

Thus, a mixture of copper nitrate and **TPA-Py** in a stoichiometric ratio of 2:1 in a mixture of DMF and methanol was refluxed for 30 min., after which the precipitate was removed and the solution slowly evaporated at room temperature to afford two kinds of crystals of the complexes **TPA-Py@Cu** and **2TPA-Py@4Cu** (see Fig. 8), respectively. In complex **TPA-Py@Cu**, a ligand is coordinated with one copper(II) in a ratio of 1:1. The central Cu exhibits a distorted tetra-coordinated geometry with N and O atoms (Cu1 – O4 = 1.798 Å, Cu1 – N4 = 2.151 Å, Cu1 – N5 = 1.859 Å and Cu1 – N6 = 1.930 Å), with an occupancy ratio 0.85: 0.15 of Cu1 and Cu1A, respectively. On the other hand, the complex **2TPA-Py@4Cu** was a self-assembly of 2 **TPA-Py** molecules, 4 copper (II) ions and 2 DMF molecules in a ratio of [ligand]:[Cu^{2+}] = 1:2, with binding to the copper cations via the N and O atoms. All bond length are typical and fall in the range 1.85-1.96 Å for Cu-O and 1.90-2.06 Å for Cu-N, respectively. The exceptions are Cu1-O4 and Cu2-O5 which are 2.77 Å and 2.51 Å, and this may be due to the presence of the unstable solvent and the intramolecular free rotations of arm units. The coordination mode of the complex **2TPA-Py@4Cu** is consistent with the spectroscopic data. More importantly, HRMS was performed (Figs. S3-S4) and confirmed two complexes with m/z = 1159.4449 for **TPA-Py@Cu** and m/z = 2589.7179 for **2TPA-Py@4Cu**, respectively, which correspond to the results obtained from the single crystal X-ray diffraction analysis. According to their crystal structure, the five-coordinate complexation with between the ligand TPA and copper (II) show higher thermodynamic complex stability. On the other hand, we compared to the atomic radius of the common metal, such as zinc (II) (74 pm), copper (II) (73 pm), nickel (69 pm), the iron (64.6 ppm)

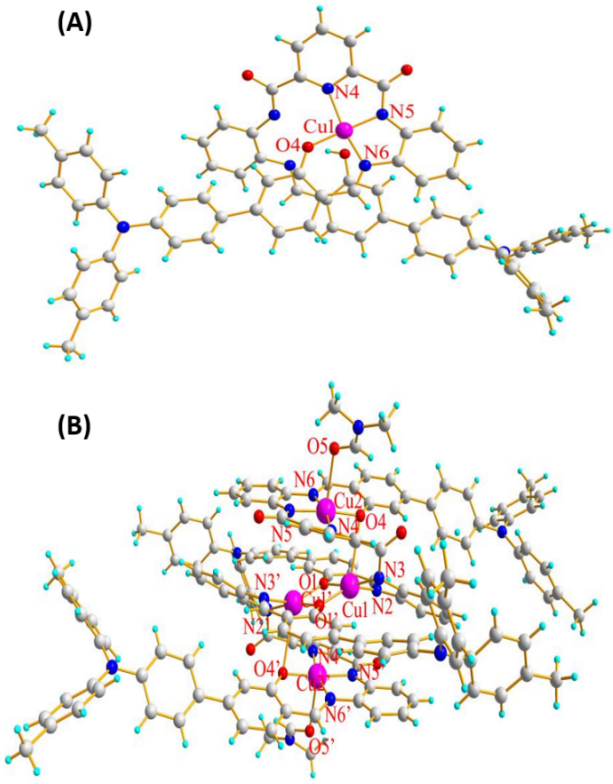

Fig. 8. X-ray single crystal diffraction image of **TPA-Py@Cu^{2+}** (A) and **TPA-Py@2Cu** (B).

According to the crystal structures of complexes **TPA-Py@Cu^{2+}** and **TPA-Py@2Cu**, as well as the ^{1}H NMR spectroscopic titration results, there are two kinds of coordination mode between the ligands and copper cations. Thus, we infer the complexes **TPA-Py@Cu^{2+}** and **2TPA-Py@4Cu** would be present in a dynamic balance in the crystallization process, because of the molecular rotation of the complex, as per the following equation:

$$\text{TPA-Py} + \text{Cu}^{2+} \rightleftharpoons \text{TPA-Py@Cu}^{2+} \qquad (1)$$

$$\text{TPA-Py@Cu}^{2+} + \text{TPA-Py} + 3\text{Cu}^{2+} + 2\text{DMF} \rightleftharpoons 2\text{TPA-Py@4Cu}^{2+}\text{@2DMF} \qquad (2)$$

The TPA can react with a copper (II) to afford the **TPA-Py@Cu^{2+}** species in dilute solution, and this balance would be destroyed on adding the extra Cu^{2+} according to Le Chatelier's principle, to achieve the thermodynamic complex **2TPA-Py@4Cu^{2+}.**

3.7 Theoretical calculations and binding mechanism

To further understand the electron delocalization and the electronic properties of ligand **TPA-Py**, and complexes **TPA-Py@Cu^{2+}** and **2TPA-Py@4Cu^{2+}**, the molecular geometries were calculated by density functional theory (DFT) using the B3LYP/6-31G(d) method in the Gaussian 16 program. The highest occupied molecular orbital (HOMO) and the lowest unoccupied molecular orbital (LUMO) orbitals of ligand **TPA-Py** were mainly located on the triphenylamine units and the bridge of the *N*, *N*'-(2-aminophenyl)-2,6-diformyl iminopyridine group, respectively. In the case of **TPA-Py@Cu^{2+}**, the HOMO was spaced over the donating group of one triphenylamine unit, the LUMO was mainly located in the electron-withdrawing group of the *N*,*N*'-(2-aminophenyl)-2,6-diformyl iminopyridine fragment and partly located in the coordination copper atom in the α molecular orbital, as for the and β molecular orbital, however, the LUMO was mostly cloud on the coordination copper atom.[46] In the tetra-ligand **2TPA-Py@4Cu^{2+},** the HOMO electrons mainly occupied both of the triphenylamine units in the α and β molecular orbitals, and the LUMO level was located in the *N*,*N*'-(2-aminophenyl)-2,6-diformyl iminopyridine in α molecular orbitals and the copper atoms on the coordinate bridge with its coordination atoms are in β molecular orbitals, respectively. Based on the theoretical calculations, an excited electron transfer route from the triphenylamine unit to the copper ions via its coordination atoms could clearly observed, and this may be attributed to the emission quenching phenomenon. The energy band gap (ΔE) between the

HOMO and LUMO of **TPA-Py**, **TPA-Py@Cu** and **2TPA-Py@4Cu** are illustrated in Tables 1 and 2.

Table 1. The HOMO and LUMO for **TPA-Py**, **TPA-Py@Cu** and **TPA-Py@2Cu**.

	TPA-Py	**TPA-Py@Cu**		**TPA-Py@2Cu**	
		α electron	β electron	α electron	β electron
HOMO(eV)	-4.88	-4.79	-4.79	-4.63	-4.62
LUMO(eV)	-1.91	-2.02	1-2.5	-1.80	-2.32
ΔE(eV)	2.97	2.77	2.64	2.83	2.30

***ΔE(eV) is the difference between HOMO and LUMO energy levels.**

Table 2. Optimized structures and HOMO/LUMO of α electron and β electron of the **TPA-Py**, **TPA-Py@Cu** and **TPA-Py@2Cu** complex by DFT calculations.

		HOMO	**LUMO**
TPA-Py		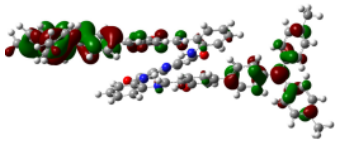	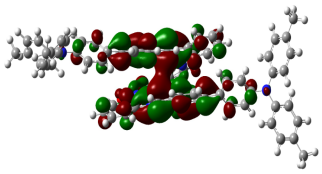
TPA-Py @Cu	**α electron**	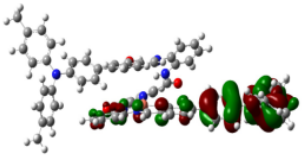	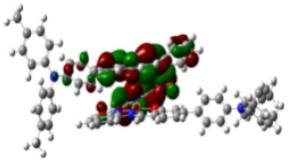
	β electron	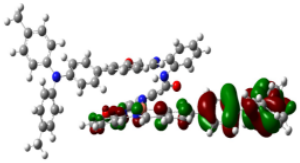	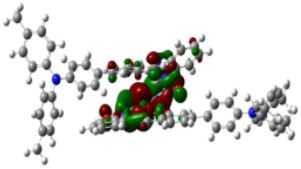
TPA-Py @2Cu	**α electron**		

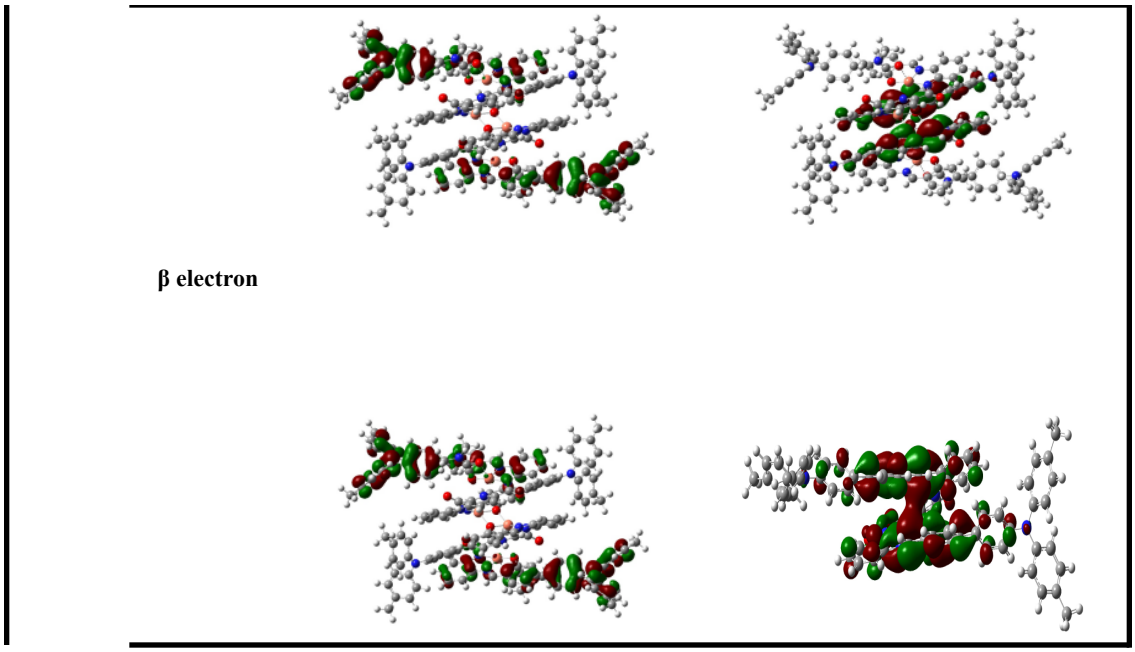

3.8 Applications

In order to further evaluate the potential applications of probe **TPA-Py** in the detection of Cu^{2+} in real specimens, water samples from artificial lake (at Guizhou Medical University) and running water (at our laboratory) were collected for testing. The fluorescence intensity of the mixture showed a remarkable decrease accompanied with a color change from bright to dark under 365 nm UV lamp irradiation. The recoveries of the probe were calculated in the range of 98.91%~101.60% for tap water and in the range of 100.43%~112.38% for artificial lake water (Table 3). The results revealed that **TPA-Py** is a sensitive and selective probe for Cu^{2+} monitoring in environmentally relevant water samples.

Table 3. Detection details of Cu^{2+} in environmental water samples

Sample	Measured ($\mu mol \cdot L^{-1}$)	Added ($\mu mol \cdot L^{-1}$)	Detected ($\mu mol \cdot L^{-1}$)	Recovery (n=3,%)	RSD (%)
Running water	9.39	5.00	14.47	101.60	0.80
		10.00	19.28	98.91	1.91
		20.00	29.38	99.95	1.06
Artificial lake	15.38	8.00	24.37	112.38	1.56
		15.00	30.86	103.20	1.43
		30.00	45.51	100.43	2.31

4 CONCLUSION

In summary, we have developed a new AIE fluorescent probe based on two triphenylamine units attached to a pyridine-2,6-dicarboxamide core, which exhibits good selectivity and sensitivity for detecting copper in a THF/H_2O mixture. Furthermore, in the presence of copper, the probe solution showed an obvious color change from yellow to brown under daylight and from bright to dark under UV lamp irradiation with a detection limit as low as 2.687×10^{-7} $mol\cdot L^{-1}$. Using titration experiments, a good linear relationship was found which may allow the probe to be utilized for the quantitative and qualitative detection of Cu^{2+} in real samples. Furthermore, the results of a single crystal X-ray diffraction confirmed that there exist two types of species between **TPA-Py** and copper ions, and their binding constants were calculated to be 4.0694×10^3 and 1.0761×10^6. The two binding modes were confirmed by absorption titration, ^1H NMR spectroscopic titrations, DFT calculations, HRMS spectra and single crystal X-ray diffraction. On the other hand, we successfully utilized the probe in the application of real water sample detection. We believe this work provides a new example of AIEgens for ion detection and provides insight into the binding modes. Such results may inform researchers in broader fields such as biometrics, and this research is on-going in our laboratory.

CONFLICTS OF INTEREST

There are no conflicts to declare.

ACKNOWLEDEGMENTS

This work was supported by and the National Natural Science Foundation of China (21975054, 21602014, 22065009, 22066007), the Guizhou Provincial Natural Science Foundation (grant

number [2019] 2792], grant number [2018] 5779-14). CR thanks the EPSRC for an Overseas Travel Grant (EP/R023816/1).

SUPPLEMENTARY DATA

Electronic Supplementary Information (ESI) available: Details of the NMR and MS spectra, the photophysical properties of the probe and the X-ray crystallography analysis data.

REFERENCES

1. Nielsen, F. H., Essential and toxic trace elements in human health and disease. *Current topics in nutrition and disease* **2008,** *18*, 277-292.

2. Mahurpawar, M., Effects of heavy metals on human health. *International Journal of Reseacrh-Granthaalayah, ISSN-23500530* **2015**, 2394-3629.

3. Uriu-Adams, J. Y.; Keen, C. L., Copper, oxidative stress, and human health. *Molecular aspects of medicine* **2005,** *26* (4-5), 268-298.

4. Araya, M.; Olivares, M.; Pizarro, F., Copper in human health. *International Journal of Environment and Health* **2007,** *1* (4), 608-620.

5. Gumpu, M. B.; Sethuraman, S.; Krishnan, U. M.; Rayappan, J. B. B., A review on detection of heavy metal ions in water–an electrochemical approach. *Sensors and actuators B: chemical* **2015,** *213*, 515-533.

6. Moghaddam, M. R.; Carrara, S.; Hogan, C. F., Multi-colour bipolar electrochemiluminescence for heavy metal ion detection. *Chemical Communications* **2019,** *55* (8), 1024-1027.

7. Upadhyay, S.; Singh, A.; Sinha, R.; Omer, S.; Negi, K., Colorimetric chemosensors for d-metal ions: A review in the past, present and future prospect. *Journal of Molecular Structure* **2019,** *1193*, 89-102.

8. Berhanu, A. L.; Mohiuddin, I.; Malik, A. K.; Aulakh, J. S.; Kumar, V.; Kim, K.-H., A review of the applications of Schiff bases as optical chemical sensors. *TrAC Trends in Analytical Chemistry* **2019,** *116*, 74-91.

9. Islam, M. M.; Hu, Z.; Wang, Q.; Redshaw, C.; Feng, X., Pyrene-based aggregation-induced emission luminogens and their applications. *Materials Chemistry Frontiers* **2019,** *3* (5), 762-781.

10. Chowdhury, S.; Rooj, B.; Dutta, A.; Mandal, U., Review on recent advances in metal ions sensing using different fluorescent probes. *Journal of fluorescence* **2018,** *28* (4), 999-1021.

11. Wu, J.; Liu, W.; Ge, J.; Zhang, H.; Wang, P., New sensing mechanisms for design of fluorescent chemosensors emerging in recent years. *Chemical Society Reviews* **2011,** *40* (7), 3483-3495.

12. La, D. D.; Bhosale, S. V.; Jones, L. A.; Bhosale, S. V., Tetraphenylethylene-based AIE-active probes for sensing applications. *ACS applied materials & interfaces* **2017,** *10* (15), 12189-12216.

13. Chen, L.; Park, S. J.; Wu, D.; Kim, H. M.; Yoon, J., A two-photon ESIPT based fluorescence probe for specific detection of hypochlorite. *Dyes and Pigments* **2018,** *158*, 526-532.

14. Sedgwick, A. C.; Wu, L.; Han, H.-H.; Bull, S. D.; He, X.-P.; James, T. D.; Sessler, J. L.; Tang, B. Z.; Tian, H.; Yoon, J., Excited-state intramolecular proton-transfer (ESIPT) based fluorescence sensors and imaging agents. *Chemical Society Reviews* **2018,** *47* (23), 8842-8880.

15. Paul, B. K.; Guchhait, N., 1-Hydroxy-2-naphthaldehyde: A prospective excited-state intramolecular proton transfer (ESIPT) probe with multi-faceted applications. *Journal of luminescence* **2012,** *132* (8), 2194-2208.

16. Hu, Z.; Zhang, H.; Chen, Y.; Wang, Q.; Elsegood, M. R.; Teat, S. J.; Feng, X.; Islam, M. M.; Wu, F.; Tang, B. Z., Tetraphenylethylene-based color-tunable AIE-ESIPT chromophores. *Dyes and Pigments* **2020,** *175*, 108175.

17. Goswami, S.; Maity, S.; Maity, A. C.; kumar Das, A.; Pakhira, B.; Khanra, K.; Bhattacharyya, N.; Sarkar, S., ESIPT based Hg 2+ and fluoride chemosensor for sensitive and selective ‘turn on’red signal and cell imaging. *RSC advances* **2015,** *5* (8), 5735-5740.

18. Kaur, B.; Gupta, A.; Kaur, N., A simple schiff base as a multi responsive and sequential sensor towards Al3+, F− and Cu2+ ions. *Journal of Photochemistry and Photobiology A: Chemistry* **2020,** *389*, 112140.

19. Wang, Y.; Hou, X.; Liu, C.; Lei, M.; Zhou, Q.; Hu, S.; Xu, Z., Highly sensitive and selective ESIPT-based near-infrared fluorescent probe for detection of Pd2+. *Inorganic Chemistry Communications* **2019,** *101*, 135-141.

20. Dai, F.; Zhao, M.; Yang, F.; Wang, T.; Wang, C., An ESIPT coupled AIE fluorescent probe for biothiols detection and imaging based on a chalcone fluorophore. *Dyes and Pigments* **2020,** *183*, 108627.

21. Wang, C.; Sun, J.; Mei, H.; Gao, F., Organic semiconductor polymer nanodots as a new kind of off-on fluorescent probe for sulfide. *Microchimica Acta* **2017,** *184* (2), 445-451.

22. Liu, J.; Zhang, H.; Dong, H.; Meng, L.; Jiang, L.; Jiang, L.; Wang, Y.; Yu, J.; Sun, Y.; Hu, W., High mobility emissive organic semiconductor. *Nature communications* **2015,** *6* (1), 1-8.

23. Wang, B.; Zhao, M.; Mehdi, M.; Wang, G.; Gao, P.; Zhang, K.-Q., Biomolecule-assisted synthesis and functionality of metal nanoclusters for biological sensing: a review. *Materials Chemistry Frontiers* **2019,** *3* (9), 1722-1735.

24. Niu, Q.; Sun, T.; Li, T.; Guo, Z.; Pang, H., Highly sensitive and selective colorimetric/fluorescent probe with aggregation induced emission characteristics for multiple targets of copper, zinc and cyanide ions sensing and its practical application in water and food samples. *Sensors and Actuators B: Chemical* **2018,** *266*, 730-743.

25. Wang, X.-Y.; Yin, H.-Q.; Yin, X.-B., MOF@ COFs with strong multiemission for differentiation and ratiometric fluorescence detection. *ACS applied materials & interfaces* **2020,** *12* (18), 20973-20981.

26. Zhang, X.; Li, G.; Wu, D.; Zhang, B.; Hu, N.; Wang, H.; Liu, J.; Wu, Y., Recent advances in the construction of functionalized covalent organic frameworks and their applications to sensing. *Biosensors and Bioelectronics* **2019,** *145*, 111699.

27. Wang, X.-N.; Zhang, P.; Kirchon, A.; Li, J.-L.; Chen, W.-M.; Zhao, Y.-M.; Li, B.; Zhou, H.-C., Crystallographic Visualization of Postsynthetic Nickel Clusters into Metal–Organic Framework. *Journal of the American Chemical Society* **2019,** *141* (34), 13654-13663.

28. Kitagawa, H.; Ohtsu, H.; Kawano, M., Kinetic assembly of a thermally stable porous coordination network based on labile CuI units and the visualization of I2 sorption. *Angewandte Chemie* **2013,** *125* (47), 12621-12625.

29. Xie, H.-F.; Yu, C.-J.; Huang, Y.-L.; Xu, H.; Zhang, Q.-L.; Sun, X.-H.; Feng, X.; Redshaw, C., A turn-off fluorescent probe for the detection of Cu 2+ based on a tetraphenylethylene-functionalized salicylaldehyde Schiff-base. *Materials Chemistry Frontiers* **2020,** *4* (5), 1500-1506.

30. Krause, L.; Herbst-Irmer, R.; Sheldrick, G. M.; Stalke, D., Comparison of silver and molybdenum microfocus X-ray sources for single-crystal structure determination. *Journal of applied crystallography* **2015,** *48* (1), 3-10.

31. Sheldrick, G. M., SHELXT–Integrated space-group and crystal-structure determination. *Acta Crystallographica Section A: Foundations and Advances* **2015,** *71* (1), 3-8.

32. Kwon, J. E.; Park, S. Y., Advanced organic optoelectronic materials: Harnessing excited‐state intramolecular proton transfer (ESIPT) process. *Advanced Materials* **2011,** *23* (32), 3615-3642.

33. Feng, Q.; Li, Y.; Li, K.; Lu, J.; Wang, J.; Fan, P.; Li, D.; Wu, D.; Hou, H., Fluorescent chemosensor for zinc ion detection with significant emission color change in aqueous solution based on AIEgen. *ChemistrySelect* **2017,** *2* (10), 3158-3162.

34. Chipem, F. A.; Mishra, A.; Krishnamoorthy, G., The role of hydrogen bonding in excited state intramolecular charge transfer. *Physical Chemistry Chemical Physics* **2012,** *14* (25), 8775-8790.

35. Hu, R.; Lager, E.; Aguilar-Aguilar, A.; Liu, J.; Lam, J. W.; Sung, H. H.; Williams, I. D.; Zhong, Y.; Wong, K. S.; Pena-Cabrera, E., Twisted intramolecular charge transfer and aggregation-induced emission of BODIPY derivatives. *The Journal of Physical Chemistry C* **2009,** *113* (36), 15845-15853.

36. Shao, Q.; Liang, K.; Ling, H.; Wang, Y.; Yan, Z.; Xia, G.; Wang, H., Tetraphenylethylene-incorporated squaraine dyes: structural and theoretical insights into the diverse emission behaviors in solution and solid state. *Journal of Materials Chemistry C* **2020,** *8* (13), 4549-4556.

37. Liu, B.; Luo, Z.; Si, S.; Zhou, X.; Pan, C.; Wang, L., A photostable triphenylamine-based flavonoid dye: Solvatochromism, aggregation-induced emission enhancement, fabrication of organic nanodots, and cell imaging applications. *Dyes and Pigments* **2017,** *142*, 32-38.

38. Yadav, S. B.; Sonvane, S. S.; Sekar, N., Novel blue-green emitting NLOphoric triphenylamine-imidazole based donor-π-acceptor compound: Solvatochromism, DFT, TD-DFT and non-linear optical studies. *Spectrochimica Acta Part A: Molecular and Biomolecular Spectroscopy* **2020,** *224*, 117421.

39. Yang, Y.; Li, B.; Zhang, L., Design and synthesis of triphenylamine-malonitrile derivatives as solvatochromic fluorescent dyes. *Sensors and Actuators B: Chemical* **2013,** *183*, 46-51.

40. Li, Y.; Tan, T.; Wang, S.; Xiao, Y.; Li, X., Highly solvatochromic fluorescence of anthraquinone dyes based on triphenylamines. *Dyes and Pigments* **2017,** *144*, 262-270.

41. Cozzi, P. G., Metal–Salen Schiff base complexes in catalysis: practical aspects. *Chemical Society Reviews* **2004,** *33* (7), 410-421.

42. Akhter, S.; Zaman, H. U.; Mir, S.; Dar, A. M.; Shrivastava, S., Synthesis of Schiff base metal complexes: a concise review. *European Chemical Bulletin* **2017,** *6* (10), 475-483.

43. Thordarson, P., Determining association constants from titration experiments in supramolecular chemistry. *Chemical Society Reviews* **2011,** *40* (3), 1305-1323.

44. Long, G. L.; Winefordner, J. D., Limit of detection. A closer look at the IUPAC definition. *Analytical chemistry* **1983,** *55* (7), 712A-724A.

45. Kumar, R.; Semwal, S.; Choudhury, J.; Srivastava, A., Heli (aza) cene: A Helical Molecular Tweezer with Tunable Intraand Inter-molecular Charge Transfer. **2017**.

46. Feng, X.; Xu, Z.; Hu, Z.; Qi, C.; Luo, D.; Zhao, X.; Mu, Z.; Redshaw, C.; Lam, J. W.; Ma, D., Pyrene-based blue emitters with aggregation-induced emission features for high-performance organic light-emitting diodes. *Journal of Materials Chemistry C* **2019,** *7* (8), 2283-2290.

TOC graphic

A dynamic coordination process could be observed by adding different amount of Cu^{2+} in the probe **TPA-Py** solution, this interesting phenomenon was confirmed by both spectral study and X-ray single crystal diffraction analysis (For Table of Contents Only).

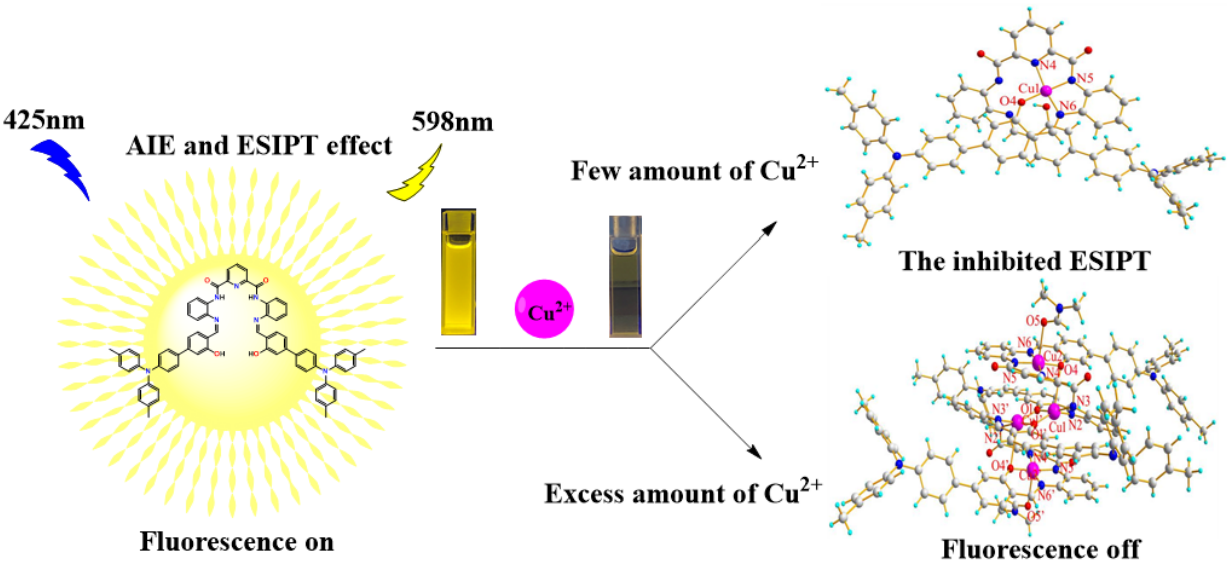

(Original type)

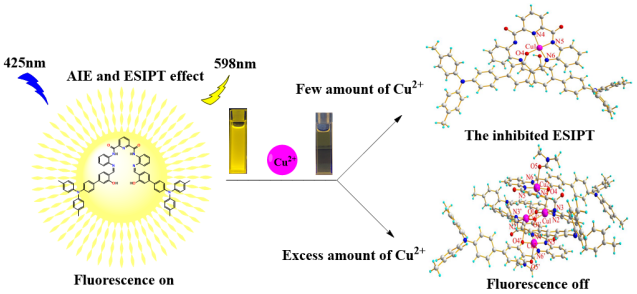

(Type 3.25 inches by 1.75 inches)